JAAS

ROYAL SOCIETY OF CHEMISTRY

PAPER

View Article Online
View Journal

Cite this: DOI: 10.1039/d6ja00127k

Towards an automated approach for rapid separation of actinides using a liquid handling system

Nicholas P. Richard, * Sean R. Scott, Christian Berry, Matthew RisenHuber, William Munley, Karen Noyes, Matt Douglas and Lori Metz

The rapid, high-precision determination of actinide isotopic compositions is critical for nuclear forensics, safeguard verification, and environmental assessment, yet these applications are often limited by multi-day chemical preparations and dependence on specialized labware. In this work, we develop a micro-scale dissolution and extraction chromatography workflow that reduces sample preparation times for U, Pu, Np, and Am to a few hours while maintaining isotopic accuracy suitable for high-precision MC-ICP-MS/MS analysis. Small-mass aliquots of geologic and reference materials (0.2–3 mg) and pre-digested SRM solutions are purified using 0.1 mL UTEVA microcolumns, with AG1-X4 and stacked UTEVA-DGA microcolumns used in separate experiments. Custom 3D-printed microcolumns and holders mounted on a repurposed liquid-handling platform deliver reagents under positive pressure, enabling rapid, automated microchemistry without a dedicated commercial extraction-chromatography system. Across a suite of NIST SRMs and glass standards, automated micro-UTEVA separations yielded U recoveries of 4–111% and Pu recoveries of 47–110%, which, although spanning a broader range, were generally lower than those obtained from manual gravity driven microcolumns (30–79% and 82–96%, respectively). Regardless, U and Pu isotope ratios from the automated separation remained within approximately 1% of certified values. Neptunium and Am recoveries were lower (typically 16–41%), highlighting areas for further optimization of the multi-actinide protocol. End-to-end workflows combining microdissolution in custom-machined well plates, 3D-printed microcolumns, and MC-ICP-MS/MS analysis were completed in under 4 hours, showing that laboratory-adaptable, platform-agnostic microchemistry on repurposed liquid-handling hardware (Hamilton MicroLab) can deliver high-quality actinide isotope ratios for time-critical nuclear forensics and safeguards.

Received 9th April 2026
Accepted 18th May 2026

DOI: 10.1039/d6ja00127k

rsc.li/jaas

1 Introduction

Since the end of the Cold War, the precise isotopic analysis of radioactive materials has become increasingly critical for scientific research and public safety, with applications across environmental systems, public health, and nuclear forensics.[1] Trace levels of radioactive elements, such as actinides, pose considerable challenges for reliable detection and measurement, necessitating advancements in analytical methods for high-accuracy isotopic characterization.[2–5] To meet this growing demand, isotope separation and analysis techniques have evolved, enabling greater precision and higher throughput across fields such as geochemistry, nuclear research, and environmental monitoring.[6–8] Chromatographic methods remain central to isotope isolation, employing gravity, syringe- or liquid chromatography (LC)-pump-driven flow, and pressure- or vacuum-assisted systems to control solvent delivery. Compared to traditional gravity methods, pumped and pressure/vacuum-based systems enable faster separations and are more compatible with automation.[9–13]

Yet even with these improvements in chromatographic hardware and throughput, time-critical applications such as nuclear forensics, safeguard verification, and environmental assessment, bulk destructive analysis remains essential for high-confidence actinide and fission-product signatures.[1] In practice, these bulk measurements are commonly supported by conventional, macro-scale sequential column chemistries, which are slow and labor-intensive, often making it challenging to achieve optimal separations within operational timelines.[14–17] These workflows can require multiple days of chemistry preparation and extensive operator intervention, which limits throughput and introduces variability. In response, some commercial systems offer automated actinide separations, but they are typically tied to proprietary hardware and rigid layouts that do not accommodate realistic sample throughputs and depend on specialized labware that may be difficult to source under urgent conditions. Under these circumstances, these

Pacific Northwest National Laboratory, 902 Battelle Blvd, Richland, WA, 99354, USA

Table 1 Summary of manual column calibration experiments

Method/reference	Matrix	Actinides separated	Approx. separation time	Typical recovery (%)
Sequential-injection TRU-resin system[18]	Nuclear waste/process solutions	Am, Cm, Pu, Th, Np, U (focus on Am, Cm, Pu)	~25 min per separation cycle for Am/C	Pu, Am: ~85–86%; other actinides (Am, U, Th, Np): typically >85–90
Stacked extraction chromatography cartridges on vacuum box[11]	Urine and related bioassay matrices	Pu, Np, Am, U, Cm	Up to 24 samples in <3 h	Chemical recoveries typically >90
Microfluidic SPE column packed with UTEVA resin[10]	8 M HNO_3	U	20–25 min from load to end of U elution	U: typically ~96–97
Tandem SPE separation on prepFast-SR system[19]	3 M HNO_3	U, Pu	Tens of minutes per sample	U: >99; Pu: >80
Hamilton MicroLab (this work)	Geologic and glass reference materials and soil-equivalent SRMs	U, Pu, Np, Th, Am	~20 min for separation; full dissolution + separation + MC-ICP-MS/MS in <4 h	U: 4–111; Pu: 47–110; Np: 16–41; Am: 16–41

systems may also depend on specialized labware with limited availability, leading to delays when replacement components must be ordered. Together, these constraints highlight the need for flexible, laboratory-adaptable microscale workflows that can be rapidly implemented on existing liquid-handling platforms, minimizing manual operations and shortening purification timelines without sacrificing isotopic accuracy.

To address the need for rapid, high-throughput actinide isotopic analysis in nuclear forensics, safeguard verification, or environmental assessment, this work presents an automated micro-scale dissolution and extraction chromatography workflow implemented on a repurposed Hamilton MicroLab liquid-handling system coupled to an MC-ICP-MS/MS (*e.g.*, the new Thermo Scientific Neoma MC-ICP-MS/MS). Custom 3D-printed microcolumns and holders are used with UTEVA, AG1-X4, and stacked UTEVA-DGA resins under positive pressure to enable rapid microdissolution and chemical purification of U, Pu, Np, and Am from small-mass aliquots of geologic materials and standard reference materials. The primary goals of this work are to develop methods that are transferable across process steps, leverage 3D-printed labware compatible with strong acids and automation on platform-agnostic hardware, and reduce the time required to purify and analyze actinide isotopic ratios by MC-ICP-MS/MS. Ultimately, by combining automated liquid handling, 3D-printed labware, and microscale chemistry, this workflow is designed to deliver rapid, high-throughput characterization of actinide particles or small particle assemblages, within the timelines demanded by nuclear forensics and safeguard applications, and at scales well below the mass range of conventional bulk methods.[1] As summarized in Table 1, existing automated actinide separation methods are frequently optimized for a single matrix type or limited to one or two actinides, with prior approaches largely tailored to urine or nuclear process solutions rather than complex matrix soil digest and geologic reference materials.[10,11,18,19] The workflow presented here addresses these limitations by targeting up to five actinides from these matrices on repurposed, platform-agnostic hardware, while maintaining accurate isotope ratios and completing the full dissolution-to-analysis pipeline in under 4 hours.

2 Experimental section

All research presented herein was carried out within the Physical Sciences Facilities of Pacific Northwest National Laboratory. The development of chemistry included three stages: calibration and testing of miniaturized gravity-based columns, transitioning gravity-based separations to the liquid-handling system (Hamilton MicroLab), and analysis of elutions on the MC-ICP-MS/MS. In addition, methods for rapid "micro-dissolutions" were developed to complement the microchemistry separations. Miniaturized column tests were conducted in the Ultratrace Laboratory, microchemistry and micro-dissolution were conducted in the Radiation Detection Laboratory, and mass spectrometry analyses were undertaken in the Material Science and Technology Laboratory. In all experiments, including manual gravity-driven calibrations, automated MicroLab separations, and microdissolution tests, actinide recoveries were calculated by comparing measured concentrations to known values for each material, unless otherwise noted for experiments in which ^{233}U was added for isotope dilution measurements. All spikes were aliquoted gravimetrically in a clean room, using calibrated balance and acid-cleaned labware, prior to dilution.

2.1 Manual gravity-driven calibration of small-volume chromatography and extraction columns

Prior to elemental purification using the Hamilton Microlab system, miniaturized column separations were performed manually under gravity-driven flow for calibration. This testing ensured that (1) chemical yields were acceptable, and (2) eluted fractions from the columns were able to be analyzed directly without further processing after separations (*e.g.*, no dry downs

Table 2 Summary of manual column calibration experiments

Column/resin	Sample(s)	Analyte	Analysis
microUTEVA 100–150 μm	NIST SRMs 1646a, 2706, 2711a, 2780a, 4350b, blank	U	^{234}U–^{235}U–^{238}U MIC[a]
microUTEVA 100–150 μm	NIST SRM 2709a spiked with CRM-137 Pu ($n = 4$), blank	U, Pu	^{234}U–^{235}U–^{238}U MIC, ^{239}Pu–^{240}Pu–^{241}Pu–^{242}Pu MIC[a]
microUTEVA 100–150 μm	NIST SRM 1646a spiked with CRM-138 Pu and ^{237}Np ($n = 4$), blank	Pu, Np	^{237}Np–^{239}Pu–^{240}Pu–^{241}Pu MIC[a]
microUTEVA 100–150 μm	NIST SRM 2709a spiked with CRM-138 and ^{233}U ($n = 3$), blank	U, Pu	^{233}U–^{235}U–^{238}U–^{239}Pu–^{240}Pu–^{241}Pu–^{242}Pu simultaneous MIC[a]-F using CO_2
microAG1-X8 100–200 mesh	NIST SRM2709a ($n = 1$)	U	^{234}U–^{235}U–^{238}U MIC[a]

[a] MIC, multiple ion counters.

or transpositions). Columns were constructed from disposable pipette tips by cutting off the reservoirs and placing 1.5 mm frits at the bottom of the columns to hold the resin in place. Approximately 0.1 mL of resin was used for each column, with resins tested including UTEVA and AG1-X4. All separation schemes were downsized relative to their "macro" counterparts, which use 2 mL Eichrom resin cartridges for UTEVA or 2 mL "homemade" columns for AG1-X4. Previously digested standard reference materials (SRMs), including NIST 1646a, 2706, 2709a, 2711a, 2780a, 4350b, 4353, 4353a, and 4354, were used for testing and calibration. The composition, category, and primary use of each SRM are listed in Table S1. Eluted fractions from these experiments were analyzed on the MC-ICP-MS/MS. A summary of these experiments is provided in Table 2. Because these environmental SRMs are not isotopic CRMs, U-isotope ratios were obtained from the literature when available (Goldstein *et al.* (2021) for NIST 4350b; Scott *et al.* (2024) for NIST 2780a) or from the GEOREM database (additional U-isotope data for NIST 4350b).[20,21] For SRMs without published U isotope data, these materials are not known to contain non-natural U; therefore, (^{234}U/^{238}U $\approx 5.4 \times 10^{-5}$, ^{235}U/^{238}U $\approx 7.20 \times 10^{-3}$) were assumed.

2.2 Microdissolution and chemistry using automated liquid handling

2.2.1 Hamilton MicroLab system. The Hamilton Microlab Prep automated liquid handler platform, initially designed for biological applications, was repurposed for the dissolution and chromatographic separation of inorganic materials, primarily actinides. Fig. 1 shows the extraction chromatography workflow, while Fig. S1 and S2 show the MicroLab Prep with both commercial and custom components labeled. Typically used for adding reagents, transferring samples, mixing, and diluting liquids, the system was adapted to meet the specialized demands of separation and purification processes as discussed below.

2.2.2 Custom designs and 3-D printing. Custom columns were designed using SolidWorks CAD software and 3D-printed from Clear V4 resin using the Formlabs 3L stereolithography 3D printer. Following printing, the parts were washed in isopropyl alcohol for 5 minutes, dried, and cured at 60 °C for 15 minutes in the Form Cure L UV curing station. Stereolithography printing achieves a layer thickness of 0.050 mm, enabling reproducible fabrication of 1 mm diameter channels. This resolution is superior to traditional fused deposition modeling 3D printing for applications requiring fine structural detail. All 3D-printed columns were used only once and replaced with freshly printed columns for each experiment; no visible degradation of the clear V4 resin was observed at any point during the study.

To optimize column flow, liquids needed to be forced through the columns, similar to the use of vacuum boxes for Eichrom resin cartridges. Initial efforts to design a comparable system included a vacuum-based setup to accommodate a full 96-rack of columns, with the capability to process all columns simultaneously. However, maintaining a sealed system for efficient vacuum was difficult, so a positive-pressure-based design was implemented. This included a 3D-printed piece with a compressed-air attachment that could be placed on top of the column plate. Vinyl tape was used to create a seal between the positive pressure piece and the column plate (Fig. S1). Column configurations were later refined to enable the collection of multiple eluted fractions in a single microtiter plate, reducing the setup to include only eight columns (Fig. S1). The positive-pressure piece was also adjusted to exclusively cover these eight columns. Positive pressure was applied *via* a single compressed-air inlet distributed across all columns simultaneously through the 3D-printed pressure piece. No noticeable edge effects were observed during operation, with outer columns exhibiting flow rates consistent with those of inner columns. A 3D-printed rack was used to hold the columns in place and to allow them to be moved manually across each collection well within the microtiter plate positioned beneath the columns. Splash-back and cross-contamination between collection wells were mitigated by several design features. For the dissolution plate, the programmable dispensing depth of the Hamilton Liquid Handler delivers reagents directly to the bottom of each well, eliminating splashback during acid addition. For the collection plate, eluted fractions were collected into a Waters 96-well polypropylene plate with 2 mL square wells and pyramid bases, with total volumes per well remaining

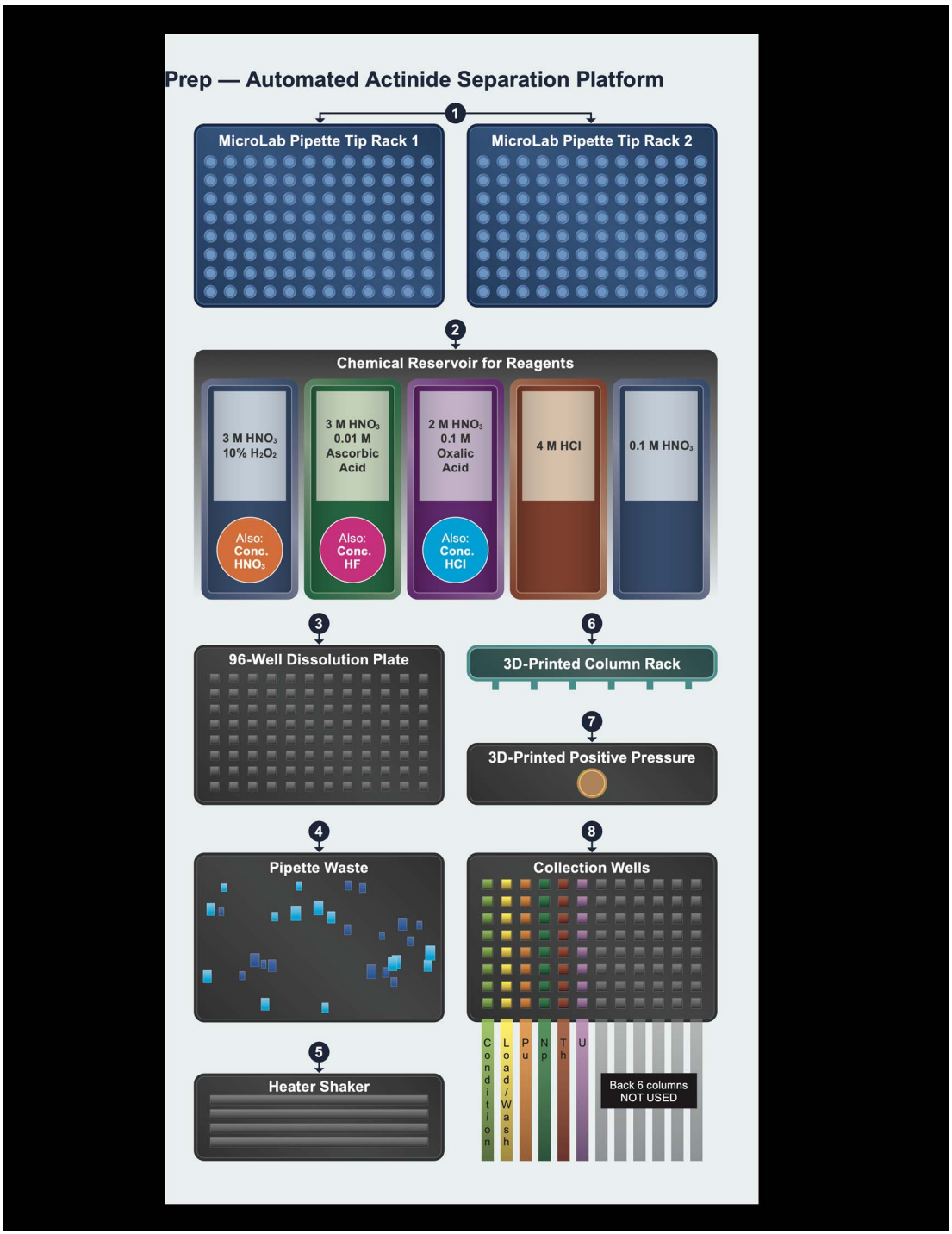

Fig. 1 Schematic of the automated microdissolution and extraction chromatography workflow implemented on the Hamilton MicroLab system. Acid addition for microdissolutions: MicroLab pipettes (1) dispense 15 μL concentrated HNO_3, 10 μL concentrated HF, and 10 μL concentrated HCl into the appropriate wells of the 96-well dissolution plate (2, 3). Pipettes are then placed in pipette waste (4) after each contact with a sample well. The plate is placed on the heat shaker (5) and heated to 105 °C, then shaken at 250–1000 rpm until the samples fully dissolve and reach dryness (~80–90 min; ~4 h for the Axygen plate). The dissolution plate is then removed from the heat shaker and returned to the deck position (3). MicroLab pipettes add 3 M HNO_3 + 10% H_2O_2 to each well, and a brief wait step allows oxidation of U, Pu, and Np to the appropriate valence states. 3D-printed columns (6) pre-packed with ~0.1 mL UTEVA, AG1-X4, or stacked UTEVA-DGA resin are conditioned with 3 M HNO_3 + 10% H_2O_2 under positive pressure (7). MicroLab pipettes (1) deliver specific chemical reagents (2) to the column (6), which is positioned above the collection wells (8). The chemical fractions are eluted under positive pressure (7) to collect the resulting eluents: Pu: 3 M HNO_3 + 0.01 M ascorbic acid; Np: 2 M HNO_3 + 0.1 M oxalic acid; Th: 4 M HCl; U: 0.1 M HNO_3; Am: from DGA after 6 M HNO_3 and 0.01 M HNO_3 steps. Fractions are collected in the collection wells (8). Actual photographs of the instrument configuration, including custom 3D-printed components and commercial accessories, are provided in the SI (Fig. S1 and S2). Actual photographs of the instrument configuration, including custom 3D-printed components and commercial accessories, are provided in the SI (Fig. S1 and S2).

Table 3 Materials used for microdissolution testing

Sample type	Description	Sample sizes
TB-Macusani	High-silica glassy geologic sample (rhyolite) containing high uranium abundance	0.8–2.3 mg
Basalt B3	Hawaiian crystalline basaltic material	0.15–0.5 mg
AGV-2G	Glass version of USGS reference material AGV-2	0.45–3.45 mg
NIST612	Glass reference material	0.9–1.55 mg

well below the 2 mL capacity across all elution steps, minimizing the risk of between-well cross-contamination.

2.2.3 Microdissolutions. Although initial chemistry experiments used pre-digested SRMs for testing, later experiments involved dissolving small aliquots of select geologic and glassy reference materials (Table 3). Aliquots of reference materials, typically ~1 mg, but ranging from 0.2–3 mg, were weighed into the custom-machined PTFE 96-well plate. Samples were weighed directly into the plate using a Mettler Toledo analytical balance (readability 0.00001 g), with the plate tared before and after each aliquot. The liquid handler was used to pipette 15 μL of concentrated (16 M) HNO_3, 10 μL of concentrated (29 M) HF, and 10 μL of concentrated (12 M) HCl into each well. The acid combination resulted in visible reactions within the well plate (Fig. 2). The plate was then transferred onto the heater/shaker plate within the MicroLab, which was heated to 105 °C and shaken at 250–1000 rpm. The combination of concentrated HNO_3–HF–HCl, small sample masses (0.2–3 mg), and a shallow well geometry greatly reduced diffusion path lengths and increased mass transfer, allowing rapid dissolution and evaporation. Samples were dissolved and reached dryness in approximately 80 to 90 minutes. Subsequently, samples were redissolved in either 3 M HNO_3 (for direct analysis) or 3 M HNO_3 + 10% H_2O_2 for column separations using the micro UTEVA protocol, with H_2O_2 to ensure an oxidizing medium and maintain U, Pu, and Np in high oxidation states prior to loading onto the resin. A commercially available and affordable well-plate (Axygen 96 well polypropylene 200 μl), relative to the custom-machined well-plate, was also tested but required significantly longer time periods to achieve dryness

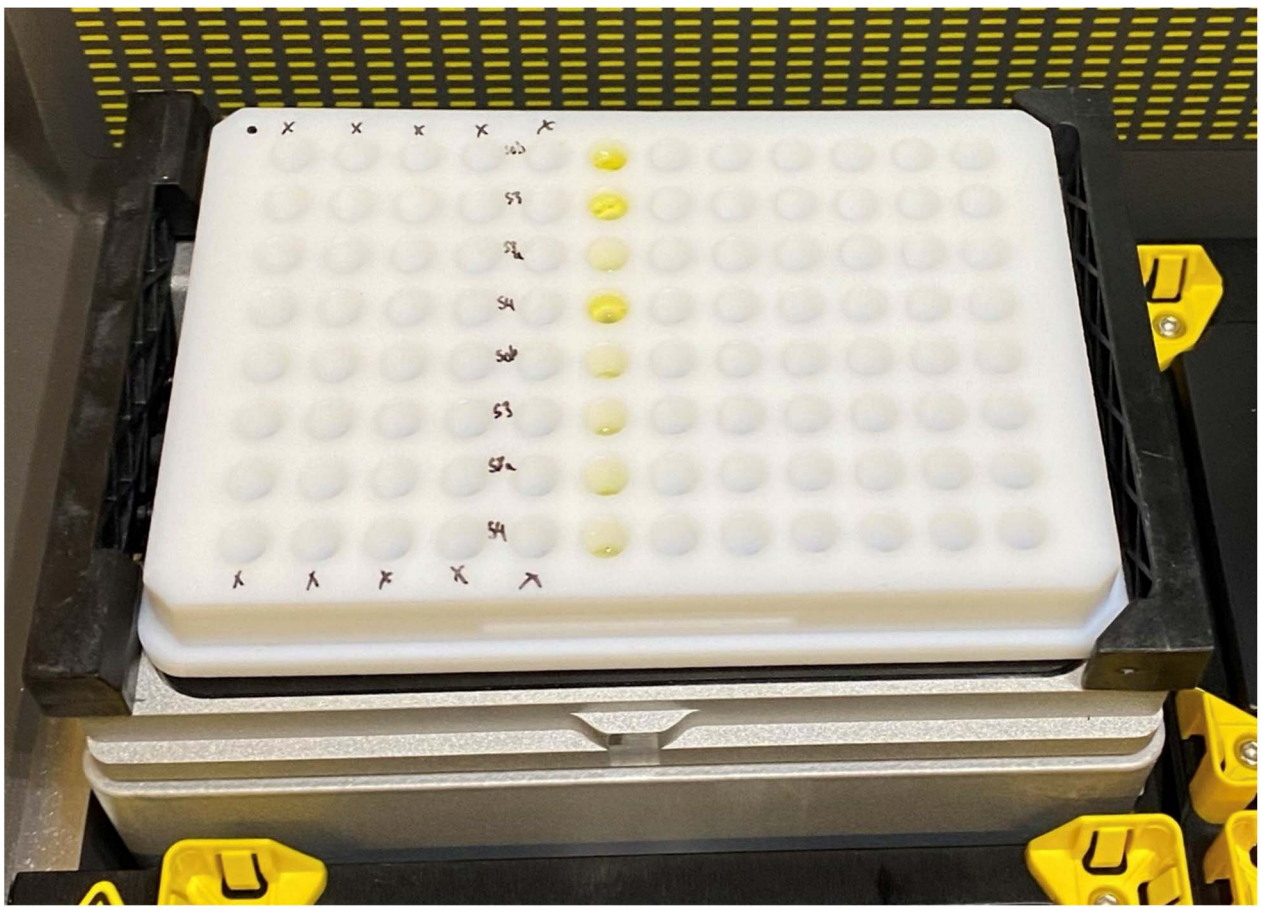

Fig. 2 Picture of the custom-machined PTFE 96-well plate on the heater/shaker during dissolution. The sixth column from the left was being used for dissolution, showing the yellow-colored acids reacting within the wells.

Table 4 Laboratory blank results for U processed through automated chemistry following microdissolution. Commercially available Axygen microtiter plates yielded U blanks compared to those from custom-machined PTFE well plates, demonstrating that neither custom 3D-printed columns nor dissolution plates introduced detectable contamination

Date	Description	U blank (pg)
05-13-2025	Automated UTEVA	2.4
05-29-2025	Automated UTEVA/DGA	25
06-26-2025	Dissolution + UTEVA blank 1	13
06-26-2025	Dissolution + UTEVA blank 2	22
06-26-2025	Dissolution + UTEVA blank 1	42
06-26-2025	Dissolution + UTEVA blank 2	3.0
07-01-2025	Dissolution + UTEVA	14
07-09-2025	Dissolution + UTEVA	0.9
07-09-2025	Dissolution + UTEVA	3.3
08-13-2025	Dissolution + UTEVA	2.1
08-13-2025	Dissolution + UTEVA	4.5
08-21-2025	Dissolution + UTEVA Axygen	45
08-21-2025	Dissolution + UTEVA Axygen	8.4

(approximately 4 hours). Process blanks were carried through the microdissolution and micro-UTEVA workflows in parallel with samples to monitor potential contamination; results are summarized in Table 4.

2.2.4 Extraction chromatography. Sequential separation of Pu, Np, Th, and U was performed on the MicroLab using micro UTEVA extraction columns or AG1-X4 columns (U only). Separation of Am additionally requires DGA resin. A frit was placed at the bottom of the 3D-printed column components, which were then preloaded with resin to the base of the reservoir (~100 μL resin volume) Each 3D-printed column consisted of a cylindrical reservoir (7 mm internal diameter, 10 mm height) connected to a narrower 8 mm-long, 4 mm-diameter stem that tapered into a 4 mm-long conical outlet terminating in a 1 mm-diameter orifice (Fig. S1). Resin slurries (UTEVA, AG1-X4, or DGA) were prepared in 2% HNO_3 and packed into the columns by pipetting 100 μL of the slurry onto a frit, followed by gentle tapping of the column to achieve a uniform, void-free bed. Excess liquid was removed by applying positive pressure. Between each liquid addition, a wait step was programmed to allow positive pressure to push the liquid through the columns.

Although many NIST SRMs are certified for U content, they may or may not contain certified or measurable quantities of Np, Pu, or Am. Accordingly, reference samples were spiked with either CRM-137 or CRM-138 (for Pu), IRMM-0243 (for Am), or ^{237}Np (for Np) before processing. NIST reference materials that do contain elevated levels of these actinides (*e.g.*, NIST 4354, 4353a, 4353) did not require spiking. To ensure equilibration during dissolution and before separation, spikes were aliquoted into well plates and dried on the heater/shaker before the samples were aliquoted.

Chemical purifications were performed on either pre-digested NIST SRMs or samples that had undergone microdissolution as described in the experimental section. For manual gravity-driven separations, sample aliquots were prepared gravimetrically, whereas for automated MicroLab experiments, pre-digested samples were handled volumetrically, with 10 μL aliquots (0.1 mg soil equivalent) used for U and Pu analyses. These aliquots were dispensed volumetrically by the Hamilton liquid handler using calibrated pipetting routines. During Np recovery optimization experiments, larger 100 μL aliquots (~1 mg soil equivalent) were used to improve detection sensitivity. The solutions were then dried on the heater/shaker prior to performing the chemical separation protocols.

Once fully dried, 0.1 mL of 3 M HNO_3 containing 10% H_2O_2 was added to the samples. The combination of oxidizing HNO_3 and H_2O_2 was selected to drive Pu and Np into well-defined, resin-compatible oxidation states prior to column loading. Specifically, H_2O_2 in 3 M HNO_3 oxidizes Pu to Pu(IV) and Np to Np(IV), both of which are strongly retained on UTEVA resin under these conditions. A five-minute wait time was programmed to allow for oxidation prior to loading onto the resin. Unlike manual methods, where agitation can be inconsistent between samples, the liquid handler ensures homogeneous oxidant contact by precisely and reproducibly delivering reagent to each well, eliminating operator-to-operator variability in reagent addition. Each extraction column containing 0.1 mL of UTEVA resin was then conditioned with two washes of 0.4 mL of 3 M HNO_3 containing 10% (v/v) H_2O_2. The dissolved samples were transferred to the columns using the liquid handler, followed by three successive 0.2 mL rinses of 3 M HNO_3 and 10% H_2O_2. Actinides were eluted sequentially as follows: Pu with 3 M HNO_3 + 0.01 M ascorbic acid, where ascorbic acid serves as a reductant, converting Pu(IV) to Pu(III), which is not retained on UTEVA and is thereby quantitatively eluted; Np with 2 M HNO_3 + 0.1 M oxalic acid, where oxalic acid acts as a Reductant, converting Np(IV) to Np(III), facilitating its selective elution; Th with 4 M HCl; and U with 0.1 M HNO_3.

When the protocol required Am isotope separation, we implemented a stacked column approach combining UTEVA and DGA resins in a vertical configuration to achieve multi-actinide separations. Dissolved samples were first passed through the stacked UTEVA-DGA column setup, with UTEVA resin performing primary actinide extraction and DGA resin enabling finer element-specific separations. Elution steps were conducted sequentially for Pu, Np, Th, and U as described above. Following U separation, Am was isolated using a two-step wash of 0.25 mL of 6 M HNO_3 followed by 0.25 mL of 0.01 M HNO_3, with the Am fraction collected in 0.01 M HNO_3.

AG1-X4 resin was also tested for U recovery from the NIST 2709a standard. The digested samples were introduced directly onto the resin and initially washed with 10 mL of 3 M HNO_3 containing 10% H_2O_2 to remove matrix components. Sequential elutions were then performed using low-molarity acid solutions specific to each actinide: Am fractions were isolated using 0.01 M HNO_3, Th using 4 M HCl, and U using 1.6 mL of 0.1 M HNO_3 for final collection.

2.2.5 Isotopic analysis. All isotopic ratio measurements were conducted on a MC-ICP-MS/MS. Analyses of multiple actinides were achieved over seventeen sessions targeting either one or multiple actinides simultaneously. Specifically, these experiments included individual measurements of U, Pu, Th,

Np, and Am, as well as simultaneous analysis of Pu–Np and U–Pu. While detector configuration were tailored for each analyte, a general description of the instrumental setup is provided below.

The Neoma MS/MS at Pacific Northwest National Laboratory (PNNL) is equipped with 11 Faraday cups in the primary array and a "nuclear" package comprised of two moveable compact discrete dynodes (CDDs) and three full-sized secondary electron multipliers (SEMs). The CDDs are attached to the L5 and L4 Faraday cups on the low and high-mass sides of the SEM array, respectively. The second SEM (SEM2) channel also contains a fixed Faraday cup that can be used when beam intensities in that channel exceed the SEM2 count-rate threshold ($\sim 2^6$ cps). The cup configuration is shown in Table S2.

Samples were introduced into the plasma using either an Apex Ω or Aridus2 desolvating nebulizer. In some cases, a dual-pass cyclonic spray chamber was used. These desolvating nebulizers (The Apex Ω and Aridus2) were used for trace-level actinide measurements to increase sensitivity and reduce solvent-derived oxide and hydride backgrounds, whereas the spray chamber was used for higher-concentration samples that did not require maximum sensitivity. The "Jet" sampler and "X" skimmer cones were used with a desolvating nebulizer system, while the standard sampler and "H" skimmer cones were used with the spray chamber and included Ni, Al, or Pt-tipped configurations. The sample introduction was automated using an Elemental Scientific μDX autosampler. Analytical parameters, including detector mass assignments, detector spacing, the number of measurements per block, and integration times, were managed through the LabBook feature within the Qtegra software. Baseline measurements were conducted on-peak before and after each sample analysis, with Qtegra automatically applying blank corrections by averaging baseline intensities and subtracting them from measured sample and standard intensities.

Specific collector configurations depended on the expected analyte concentrations within the samples, which included the use of either the ion counting array or a combination of Faradays and ion counters. Prior to each analytical session that used multiple ion counters, a ^{232}Th solution at 10 ppt was analyzed to assess ion-counter yields. Yield factors for each detector were calculated by comparing the measured ^{232}Th signal intensity to the signal intensity recorded on a Faraday cup. These yield factors were applied to normalize isotope signals, correcting for systematic differences in detector response.

Tuning parameters for the MC-ICP-MS/MS were adjusted during each session to optimize performance. Adjustments included settings for the desolvating nebulizers, where both nitrogen and argon flow rates were fine-tuned to ensure stable operation. The pre-cell mass filter (Wien filter) was also calibrated for each session, with magnetic and electrostatic fields adjusted to maximize ion transmission. For actinide measurements, the B field was typically set to 10% and the E field varied from ~40 to 50 volts. Although the MC-ICP-MS/MS is equipped with a collision reaction cell, gases were only introduced during the analytical sessions that focused on simultaneous U/Pu analysis (as described in Scott *et al.*, 2026).[21] Regardless of the use of gases, electrical potentials were tuned in the cell. The sensitivity of the ICP-MS system was further optimized by adjusting torch position, as well as altering the cool gas flow, auxiliary gas flow, and nebulizer flow parameters. All tuning parameters were optimized at the start of each analytical session to achieve maximum sensitivity and signal stability for the actinide masses of interest, using conditions similar to those described in Scott *et al.* (2026).[21] Isotopic ratios were corrected for instrumental mass bias using sample-standard bracketing with measurements of known reference standards interspersed between samples throughout each analytical session. In the following sections, our objective is to both quantify actinide recoveries across the different manual and automated workflows and determine whether these workflows maintain accurate U isotope ratios relative to certified values.

3 Results and discussion

Several experiments were conducted throughout this research, including gravity-driven column calibrations, automated dissolutions, and automated column purifications using the Hamilton MicroLab, which were validated using isotopic analysis on the MC-ICP-MS/MS. Thorough evaluation of the diverse separation methods tested here required several hundred individual analyses. Detailed results of each experiment and analysis are provided in the SI data file; key results are summarized here (Tables S3–S5). Uncertainties for all isotopic measurements are reported as 2σ standard deviations in Tables S3–S5. Actinide recoveries discussed here were determined by comparing measured concentrations to expected values based on certified reference material compositions, using external calibration unless specifically noted as isotope-dilution mass spectrometry.

3.1 Calibrations of gravity-driven microcolumns

Gravity-driven microcolumn experiments using UTEVA and AG1-X4 resins were conducted to evaluate the efficiency of actinide separations and quantify recovery rates of actinides from SRMs. The primary objectives included determining U isotope ratios (^{233}U/^{238}U, ^{234}U/^{238}U, ^{235}U/^{238}U, and ^{236}U/^{238}U) alongside isotopic ratios of Pu (^{240}Pu/^{239}Pu, ^{241}Pu/^{239}Pu, and ^{242}Pu/^{239}Pu) and Np (^{237}Np/^{239}Pu). Results from these experiments were used to compare calibrations of microchemical techniques between gravity-driven and automated purifications using the MicroLab. In the initial experiments, U was purified with UTEVA resin from multiple NIST SRMs to evaluate isotopic ratios and recovery rates. Uranium recovery ranged from 30% to 75% (Fig. 3). The isotopic ratios of U measured on the ion counting array yielded values consistent with natural U, with ^{234}U/^{238}U from 5.15×10^{-5} to 6.12×10^{-5} and ^{235}U/^{238}U from 7.26×10^{-3} to 7.29×10^{-3}. Measured ^{233}U/^{238}U and ^{236}U/^{238}U were not detected, with values $< 2 \times 10^{-7}$ and $< 3 \times 10^{-6}$ (without hydride correction), respectively, as expected considering the low U concentration in measured solutions. Across all NIST soil and sediment SRMs analyzed measured ^{235}U/^{238}U ratios ranged from 7.17×10^{-3} to 7.30×10^{-3} and ^{234}U/^{238}U

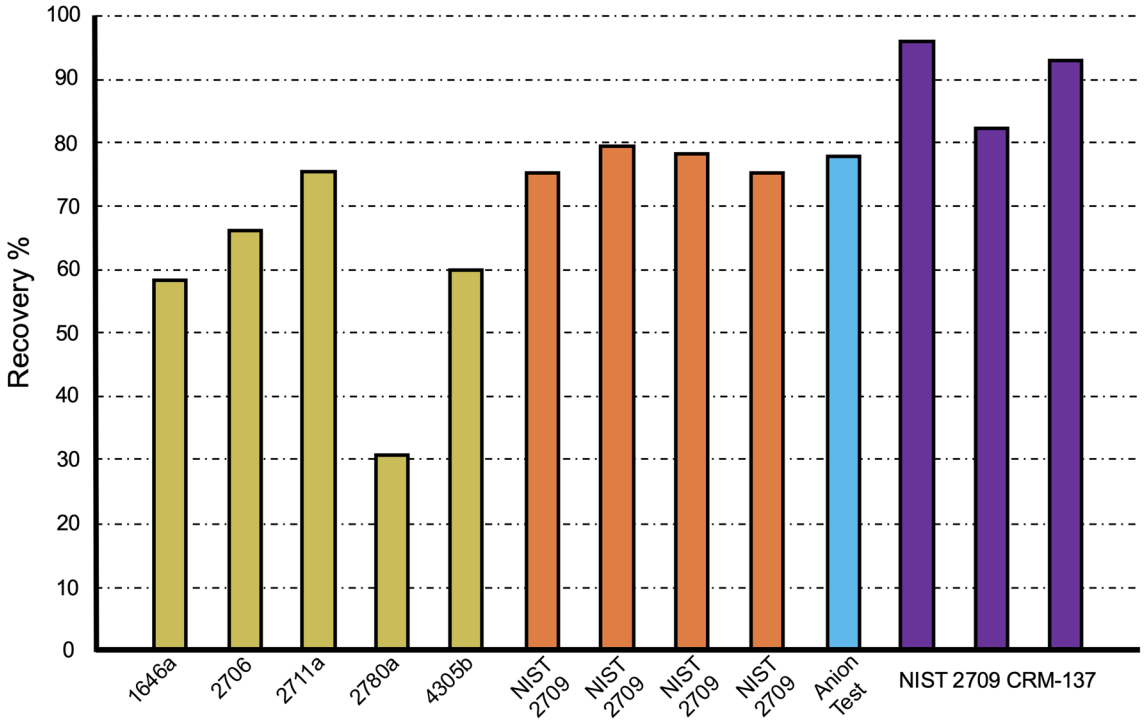

Fig. 3 Uranium and Pu recoveries for gravity-driven experiments using UTEVA and AG1-X4 resins to purify U from various NIST SRMs and three aliquots of NIST 2709a spiked with CRM-137 for Pu recovery.

from 5.15×10^{-5} to 6.33×10^{-5}, overlapping the adopted reference value within ≤1% relative. Thus, within our analytical precision, all SRMs analyzed here contain U with essentially natural isotopic compositions.

Subsequently, an experiment using NIST SRM 2709 demonstrated higher, more consistent U recovery rates of 75–79% (Fig. 3). Uranium isotope ratios were again consistent with natural U. Three NIST2709a aliquots were spiked with CRM-137 at concentrations of 10, 30, and 100 fg to evaluate Pu isotope ratios and recovery rates. Pu recovery rates ranged from 82 to 96% for the respective spike concentrations (Fig. 3). Plutonium isotopic ratios were measured as follows: $^{240}Pu/^{239}Pu$ ratios of 0.251, 0.235, and 0.248; $^{241}Pu/^{239}Pu$ ratios of 0.013, 0.0046, and 0.0053; and $^{242}Pu/^{239}Pu$ ratios of 0.0168, 0.0155, and 0.161 for the respective spikes. These values were consistent with expected values for CRM-137, although at 10 fg total Pu, the ^{241}Pu beam intensity was too low to provide an accurate measurement.

An additional experiment was conducted to evaluate the co-separation of Np and Pu. These experiments included pre-digested NIST SRM 1646a spiked with 1.2 fg, 1.1 fg, and 1.2 fg of ^{237}Np, along with 245 fg, 226 fg, and 316 fg of CRM-138, respectively. Neptunium and Pu were eluted together in the same vial and then measured using the ion counting array with ^{237}Np on CDD2 and ^{239}Pu, ^{240}Pu, and ^{241}Pu measured on the three SEMs. Expected $^{237}Np/^{239}Pu$ values ranged from 0.0041 to 0.0053, and measured values were 0.0026 to 0.0037. While the absolute values were offset low relative to the expected values, the relative differences between the samples were maintained.

Co-elution of U and Pu was also performed by collecting the U and Pu fractions within the same vial. This experiment included aliquots of predigested NIST2709a that provided ~8 ng of U and were spiked with ~43 fg of Pu (CRM-138) and ~58 pg of ^{233}U for isotope dilution. The intention of this experiment was to provide samples with $^{233}U/^{235}U$ ~1 and $^{239}Pu/^{238}U$ ~0.0007 such that the Pu isotopes could be measured on the ion counting array while U isotopes, measured as oxides using CO_2 in the collision cell, could be measured on Faraday cups. Raw isotope ratios (not corrected for any fractionation) gave $^{233}U/^{238}U$ ~1.16, $^{235}U/^{238}U$ ~0.0072, and $^{239}Pu/^{238}U$ ~0.0008.

Lastly, a gravity-driven column containing AG1-X4 resin was tested to allow for easy testing and comparisons with later work on the MicroLab. An initial purification of a single aliquot of NIST2709a resulted in a U recovery of 78% (Fig. 3). Three subsequent purifications produced U isotopic ratios consistent with natural U, with $^{235}U/^{238}U$ ~0.0072 and $^{234}U/^{238}U$ ~5.36×10^{-5}.

3.2 Integration of microchemistry

This section summarizes automated microcolumn performance for a core set of pre-digested set of NIST SRMs, focusing on how resin type, column design, and stacking configuration affected U and Pu recoveries, with preliminary Np and Am results that will be examined in greater detail in a follow-up study. These automated separations relied on custom 3D-printed microcolumn hardware, which enabled reproducible small-volume resin beds and pressure-driven flow on a repurposed liquid-handling platform. A series of microchemical experiments used AG1-X4, UTEVA, and DGA resins to evaluate recovery rates, isotopic ratios, and overall efficiency within automated

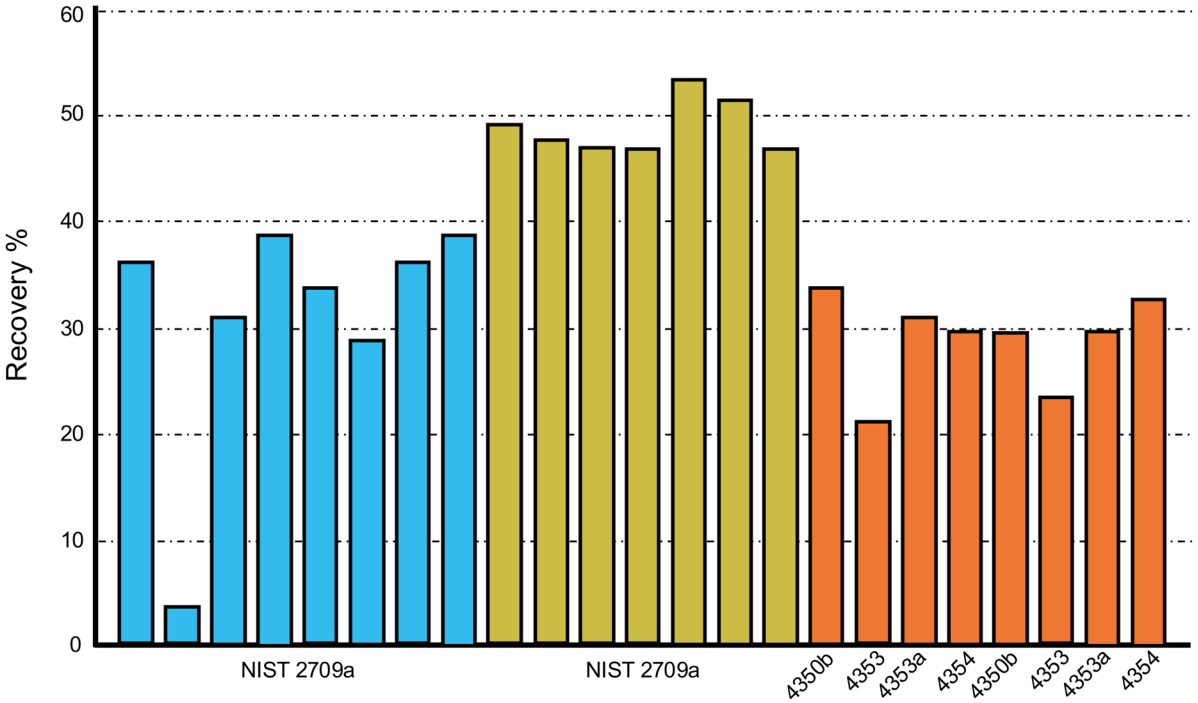

Fig. 4 Uranium recoveries from NIST 2709a during MicroLab experiments were obtained using AG1-X4 and UTEVA resins. Uranium recoveries from NIST 4305b, 4353, and 4354 were obtained using only the AG1-X4 resin.

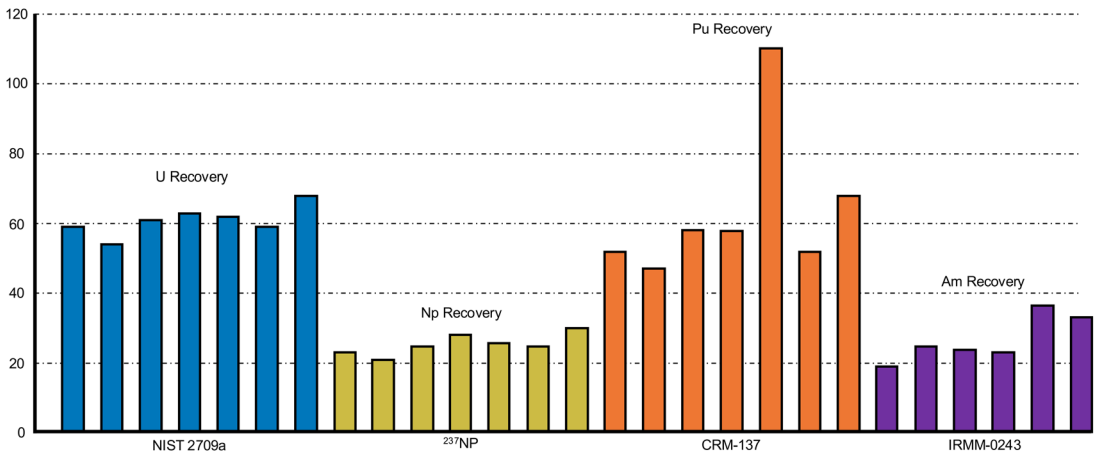

Fig. 5 Recoveries of U, Pu, Np, and Am from the double-stacked UTEVA/DGA experiment.

workflows. The automated microchemical purification experiments were performed before the incorporation of microdissolution, which were later combined with microchemistry to streamline actinide isolation and sample analysis.

Automated microcolumn experiments were conducted primarily using NIST 2709a, with a small subset of additional SRMs used to confirm transferability of the method. Initial experiment, using AG1-X4 resin produced highly variable and lower recoveries than those in the gravity test, ranging from 4% to 39%, prompting a transition to UTEVA resin, which produced more consistent U recoveries, ranging from 46% to 53% (Fig. 4). A follow-up experiment using the same methods as the initial AG1-X4 resin experiment, with two samples each of NIST 4350b, 4353, and 4353a, yielded U recoveries between 21% and 34%; full results for these materials are provided in the SI Table S4. U isotope ratios for both resins were consistent with natural U across all experiments, with $^{235}U/^{238}U$ values ranging from 7.17 $\times 10^{-3}$ to 7.30 $\times 10^{-3}$ and $^{234}U/^{238}U$ values between 5.43 $\times 10^{-5}$ and 6.33 $\times 10^{-5}$.

Building on the single-resin microcolumn tests, the workflow was next extended to a double-stacked UTEVA/DGA configuration for simultaneous separation of U, Pu, Np, and Am from NIST 2709a spiked with ^{237}Np, CRM-137, and IRMM-0243. Uranium recoveries ranged from 54% to 68%, Pu

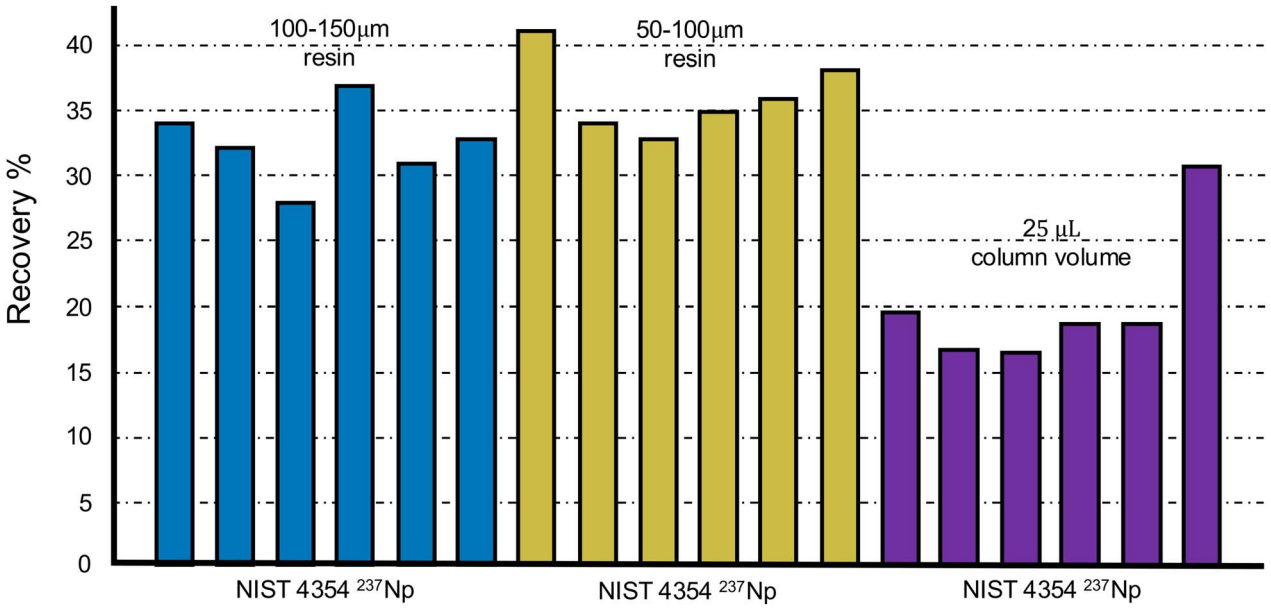

Fig. 6 Recovery of Np with varying UTEVA resin particle sizes and column volume.

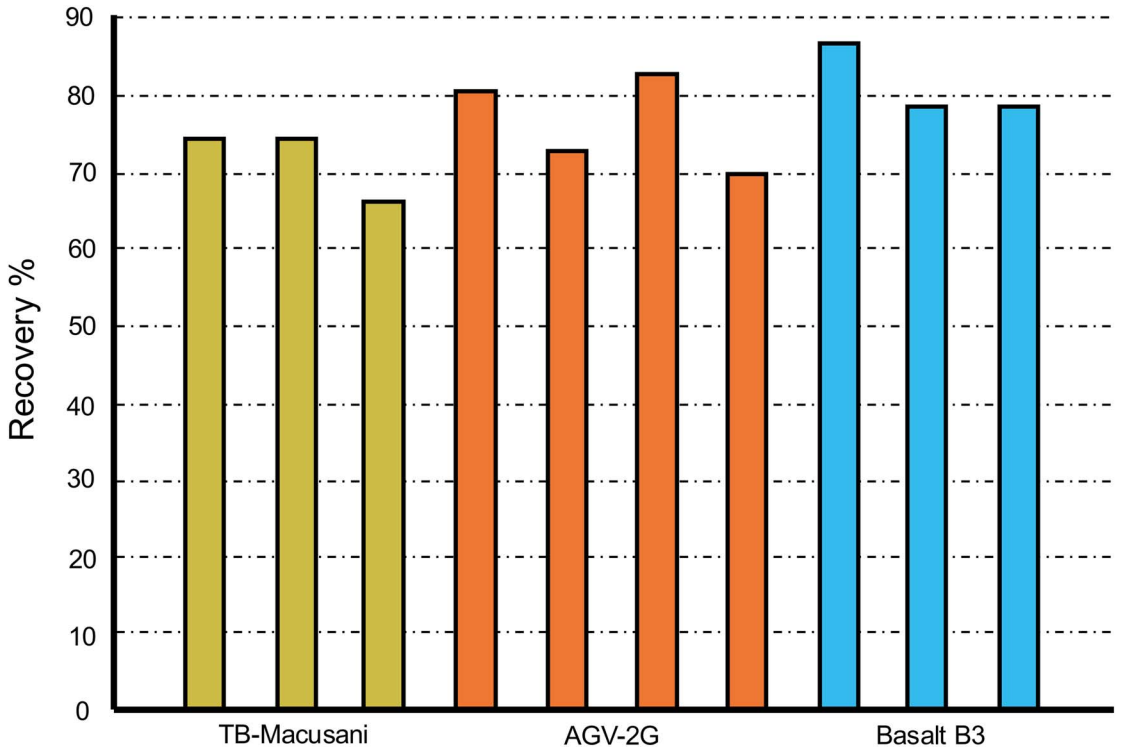

Fig. 7 Uranium recovery from micro-dissolution experiments using geologic glassy materials and samples. The graph includes data for three Basalt B3 samples, while the remaining three are excluded due to their extremely low recovery rates of <1%.

recoveries varied between 47% and 110%, Am recoveries were between 19% and 37% and Np recoveries between 21% to 30% (Fig. 5). To evaluate potential improvements in Np recovery, the effects of resin particle size and column volume were tested. No significant impact of resin size was observed, while smaller column volumes resulted in lower yields, with Np recoveries ranging from 16% to 41%, across all conditions (Fig. 6). These consistently low yields indicate that further testing and optimization are necessary to identify and address the underlying limitations affecting Np recovery in the automated method. Regardless, the double-stacked UTEVA/DGA column configuration demonstrates promise for improving multi-actinide

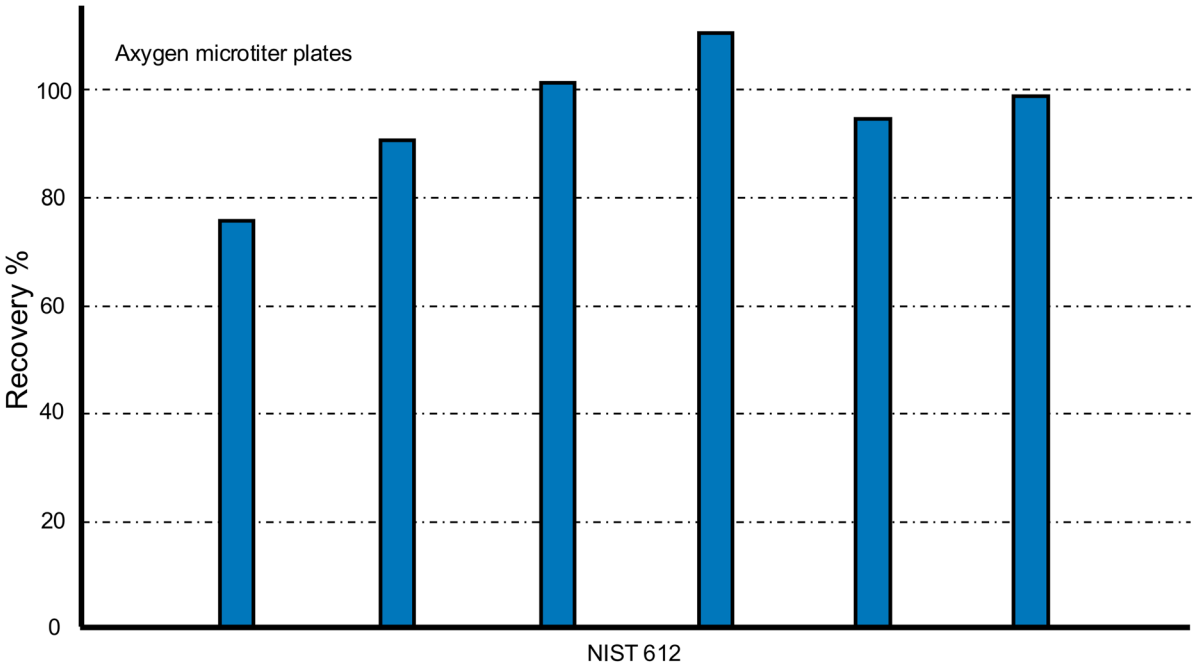

Fig. 8 Uranium recoveries from NIST 612 glass following dissolution using Axygen microtiter plates.

separations, but additional work is required to achieve higher yields for both Np and Am.

3.3 Microdissolution for direct isotopic analysis and for microchemistry

The goal of these experiments was to demonstrate that microdissolution yields both accurate U isotope ratios and acceptable U recoveries, whether used as a stand-alone sample preparation or as a front-end to micro-UTEVA separation, using a representative set of geologic glass and rock reference materials. Microdissolution was initially tested on TB-Macusani glass, with samples analyzed directly for U isotope composition without prior chemical separation. Isotopic analysis yielded $^{234}U/^{238}U$ ratios between 5.51×10^{-5} and 5.63×10^{-5} and $^{235}U/^{238}U$ ratios from 7.30×10^{-3} to 7.32×10^{-3}; consistent with expected values In the second experiment, additional aliquots of TB-Macusani glass were dissolved and then purified using UTEVA resin, producing comparable isotopic ratios ($^{234}U/^{238}U$: 5.45×10^{-5} to 5.52×10^{-5}; and $^{235}U/^{238}U$: 7.25×10^{-3} to 7.27×10^{-3}).

To assess method transferability across sample types, three additional geologic materials were tested: TB-Macusani, AGV-2G, and Basalt B3. Across these materials, U recoveries determined by ^{233}U isotope dilution ranged from 64% to 85%, with isotope ratios consistently within the uncertainty of the certified values (Fig. 7 and Table S5). The three Basalt B3 samples that yielded recoveries below 1% are excluded from Fig. 7; their results are provided in the SI (Table S5) and are likely due to incomplete dissolution of the crystalline matrix or improper column packing.

In the final microdissolution experiment, the custom-machined PTFE 96-well plate was replaced with a commercially available Axygen polypropylene plate to evaluate whether comparable performance could be achieved at lower cost. Six samples of NIST 612 glass underwent dissolution chemistry in Axygen microtiter plates. Uranium recoveries ranged from 76% to 111% (Fig. 8). The measured U isotope ratios were consistent across samples, with $^{234}U/^{238}U$ ranging from 1.25×10^{-5} to 2.48×10^{-5} and $^{235}U/^{238}U$ from 2.39×10^{-2} to 2.40×10^{-3}. Thus, the commercial Axygen plate provides a viable, cost-effective alternative for routine microdissolution work.

3.4 Isotopic accuracy

Although the manual methods generally achieved higher recoveries in most cases, the automated chemistry and dissolution experiments demonstrated comparable performance for isotopic composition analysis. The higher recoveries observed in manual separation are likely due to longer interaction times between the resin and the solution. In contrast, the automated chemistry, with its positive-pressure system and smaller column volumes, may limit the time required for complete resin-solution interaction. Despite variations in recovery, the automated method showed no significant difference in isotopic ratios when compared to the manual method (Fig. 9 and 10). Thus, the automated method is preferred for uranium isotopic analysis, given its significantly higher throughput compared to traditional manual methods and its ability to produce consistent isotopic ratios, consistent with prior work showing UTEVA-based extraction chromatography provides effective removal of common matrix cations from environmental samples without measurable alteration of U isotope ratios.[22] Similar to U, manual separation yielded higher Pu recovery rates, likely due to the longer resin-solution interaction times during the manual process. Despite lower recoveries, the Pu isotope ratios measured following the automated method with UTEVA resin are consistent with those expected in SRMs. Complete isotopic

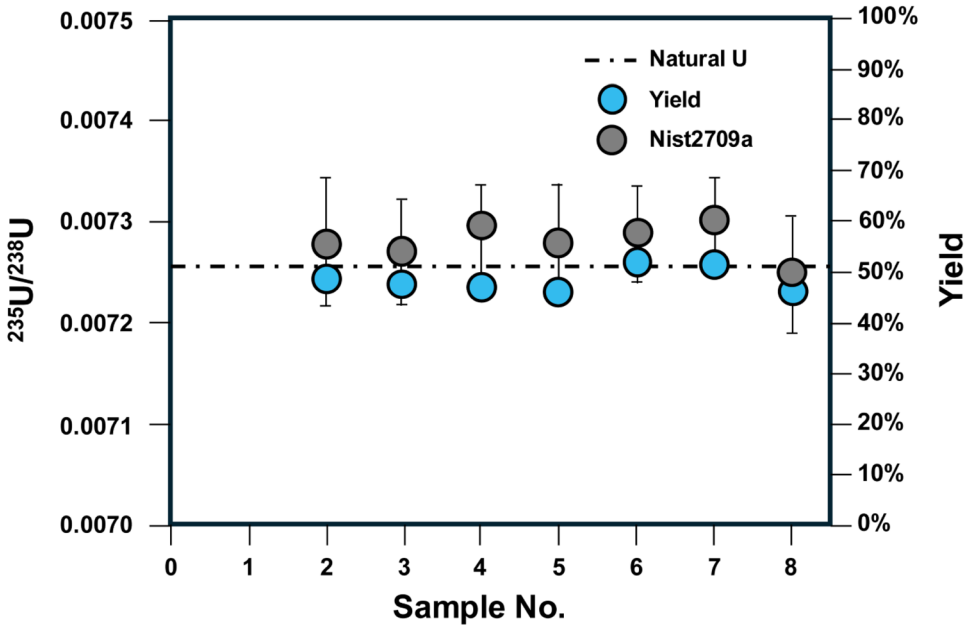

Fig. 9 $^{235}U/^{238}U$ isotopic ratios and U yield percentages plotted against sample numbers for processed NIST 2709a SRMs using the automated method. The black dashed line represents the natural $^{235}U/^{238}U$ ratio, while green circles represent the yield percentages (right axis) and grey circles the $^{235}U/^{238}U$ isotopic ratios (left axis).

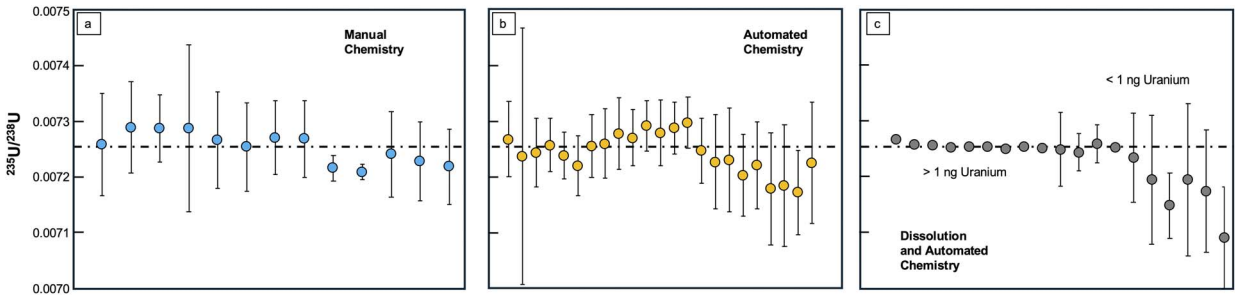

Fig. 10 $^{235}U/^{238}U$ isotope ratios obtained through (a) manual chemistry, (b) automated chemistry, and (c) dissolution followed by automated chemistry. The dashed black line represents the natural $^{235}U/^{238}U$ isotope ratio. Data for $^{235}U/^{238}U$ isotope ratios are detailed in Tables S3–S5.

ratios and associated 2σ uncertainties for all manual and automated experiments are provided in Tables S3–S5 of the SI.

3.5 Integration and modification of the Hamilton MicroLab system

A concern throughout method development was that the use of custom materials, including 3D-printed columns and a custom-machined PTFE 96-well plate, could introduce contaminants and compromise the isotopic integrity of samples during actinide measurements. To evaluate this risk, laboratory blanks were processed through the full microdissolution and automated chemistry workflow in parallel with samples (Table 4). This risk was addressed by processing laboratory blanks alongside dissolution experiments (Table 4). As shown in Table 4, contamination from these materials was not detected. Demonstrating that additively manufactured microcolumns and custom dissolution plates can be integrated into strong-acid actinide workflows without measurably impacting isotopic measurements.

A further practical consideration was the cost associated with the custom-machined PTFE well plate. To reduce costs, a later experiment used commercially available Axygen microtiter plates instead of the custom design. Sample recovery remained consistent, indicating no significant impact from switching to the lower-cost plates; further work will therefore use this lower-cost commercial plate as the primary dissolution platform while retaining 3D-printed columns for flexible microchemistry.

3.6 Timelines for actinide separation and recovery

To discuss the timing of these experiments, from chemical separation to analysis and dissolution to analysis, we first describe the co-separation of U and Pu from NIST-2709a (uranium source) spiked with CRM-138 (plutonium source) using the automated chemistry system. This is followed by

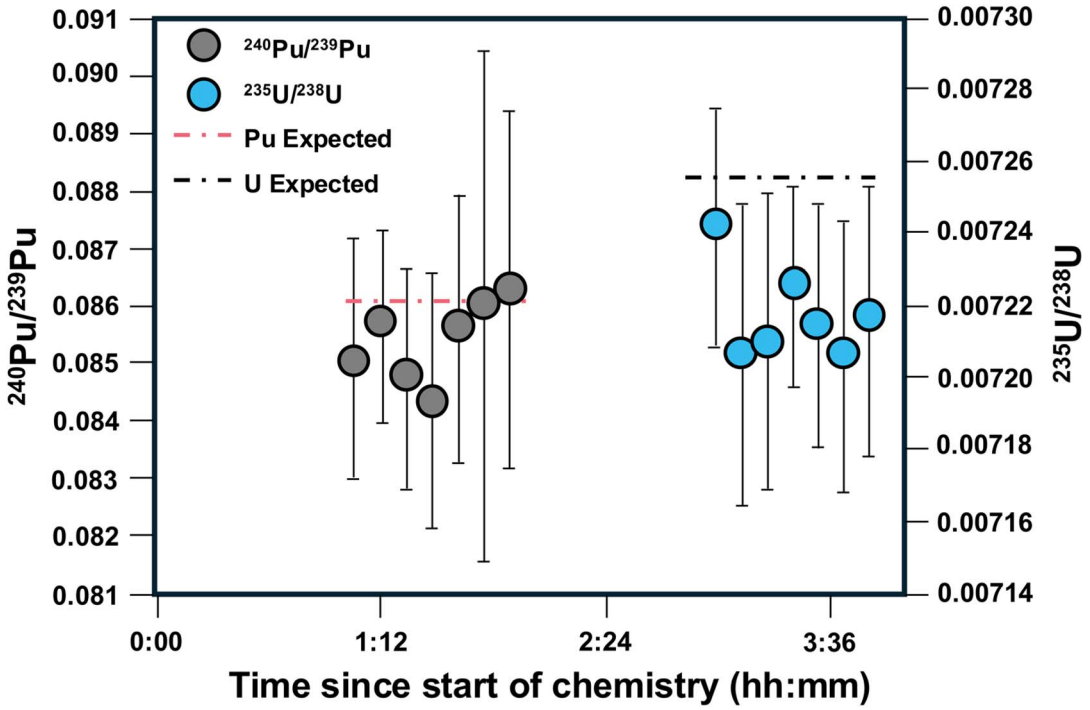

Fig. 11 $^{240}Pu/^{239}Pu$ and $^{235}U/^{238}U$ *versus* time since the start of chemical processing of NIST-2709a spiked with CRM-138 to the completion of analysis. Dashed lines represent the expected values for $^{240}Pu/^{239}Pu$ and $^{235}U/^{238}U$.

direct transfer of the purified sample fractions to the MC-ICP-MS/MS autosampler for isotopic measurement (Fig. 11). Following this, we discuss the timeline for the complete dissolution, purification, and isotopic analysis of six TB-Macusani samples (Fig. 12). It is important to note that timing began at the chemical purification step or dissolution

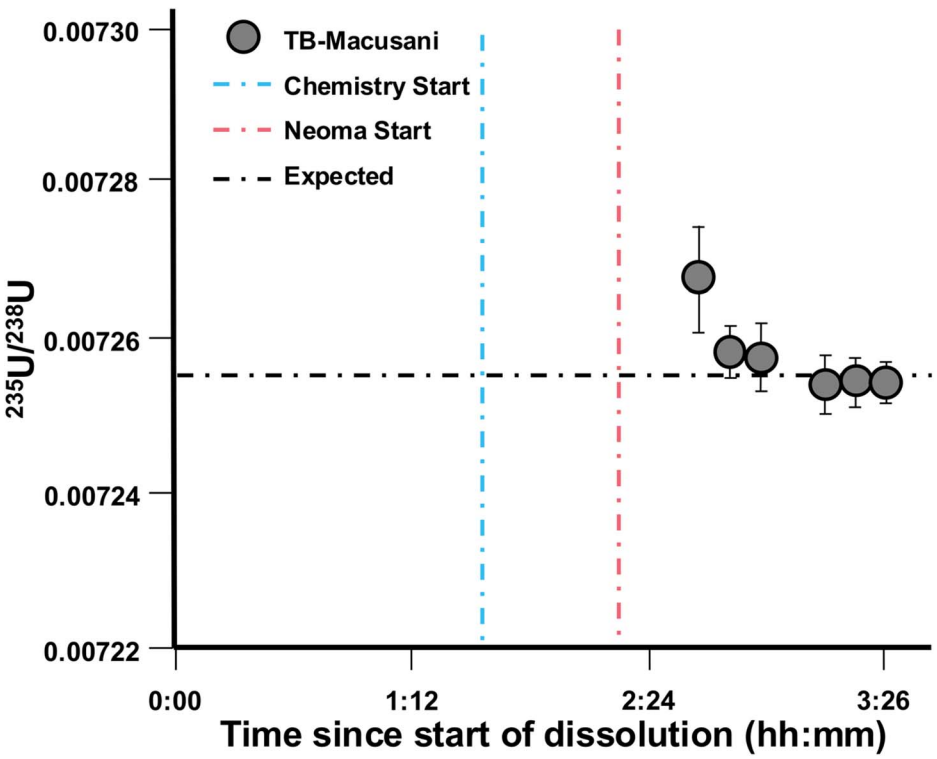

Fig. 12 Plot of $^{235}U/^{238}U$ ratios *versus* time for the dissolution of TB-Macusani glassy material through to completion of analysis on the MC-ICP-MS/MS. The black dashed line indicates the expected $^{235}U/^{238}U$ ratios, while the green dashed line shows the start of the chemistry, and the orange dashed line represents the beginning of MC-ICP-MS/MS measurements. Time zero corresponds to the beginning of dissolution.

step and does not include weighing out samples, preparing columns, or making acid solutions.

Fig. 11 compares the expected and measured $^{240}Pu/^{239}Pu$ ratios from CRM-138 and $^{235}U/^{238}U$ ratios from NIST 2709a across six samples. Good agreement was observed for the $^{240}Pu/^{239}Pu$ ratios in all samples, while only one U measurement was within analytical error of the NIST 2709a value. However, the $^{235}U/^{238}U$ ratio was within 1% of the expected value, consistent with results obtained using similar analytical procedures in previous work.[1] The purification process required approximately 20 minutes, and Pu isotope analysis of the samples was initiated at 1 hour and 11 minutes. The gap between the end of purification and the beginning of sample analysis is due to instrument setup time, including analysis of standards. Uranium isotope measurements began at approximately the 3-hour mark and concluded at about 3 hours and 40 minutes. Compared to manual methods, this automated workflow is approximately 4 times faster, reducing analysis time from multiple days to about 4 hours while maintaining accuracy in Pu and U isotope analysis.

Fig. 12 shows the measured $^{235}U/^{238}U$ ratios for TB-Macusani glass samples (~1 mg each). Dissolution was completed in approximately 90 minutes, followed by sample purification, which began immediately after dissolution at approximately 1 hour and 33 minutes. Purification required an additional 45 minutes, and isotopic measurements were completed in about 1 hour and 10 minutes. For five of the six samples analyzed, the measured $^{235}U/^{238}U$ ratios are within error of the expected values, with one sample exhibiting a slightly elevated ratio. Although U recoveries were lower than those obtained with manual methods, the isotopic ratios for most samples remained consistent with expected values. The full workflow, including dissolution, purification, and analysis, was completed in under 4 hours.

4 Conclusions

The Hamilton MicroLab system was repurposed for actinide dissolution and purification, demonstrating high-throughput capabilities for isotopic analysis. Below, we summarize the key findings from these experiments:

(1) Manual methods generally achieved higher actinide recovery yields (30% to 96%) due to longer resin-solution interaction times, whereas the automated workflow, including dissolution, produced a wider overall range (4% to 111%). Although the automated approach occasionally yielded recoveries exceeding those from manual methods, most automated results were lower, with substantial overlap between the two techniques. Despite this, the automated workflow provides sufficient recoveries for routine analytical applications and demonstrates consistency with manual results, while maintaining U and Pu isotopic ratios within ~1% of certified values.

(2) Laboratory blank tests confirmed that custom 3D-printed columns and custom-machined PTFE plates did not introduce contaminants or compromise isotopic measurements in strong-acid microdissolution and microcolumn workflows. Importantly, switching to commercially available Axygen microtiter plates significantly reduced costs without affecting sample recovery.

(3) The automated system enabled rapid dissolution and purification, completing the full U and Pu isotope analysis workflow in less than 4 hours. By contrast, manual methods may require multiple hours for chemical separation alone, often resulting in total processing times that exceed those of the automated workflow.

(4) Dissolution, purification, and analysis of six TB-Macusani glass samples were completed in less than 4 hours, and isotopic ratios for all samples remained within 1% of expected values.

(5) Automated separations achieved lower recoveries than manual methods, likely attributed primarily to reduced resin-solution contact times under positive pressure. To improve yields, particularly for Np and Am, future work will incorporate programmed wait steps or reduced flow rates during key loading and elution steps. Additionally, pressure-driven flow through small-volume resin beds may promote preferential flow channeling, where solution migrates non-uniformly through the bed, reducing effective resin-solution contact.

Given the comparable recovery, validated performance of platform-agnostic 3D-printed labware, low contamination in processed blanks, and rapid turnaround time, the Hamilton MicroLab platform is well-suited for studies requiring fast, reliable isotopic analysis. Overall, these elements allow for time-sensitive applications in environmental monitoring, public health response, and nuclear forensics, where analytical speed, consistency, and low procedural background are critical.

Author contributions

Nicholas Richard conceptualization, data curation, methodology, formal analysis, investigation, visualization, writing – original draft Sean R Scott: conceptualization, methodology, formal analysis, writing – original draft, Christian Berry: methodology, writing – original draft, Sara Mastromarino: conceptualization, writing – review & editing, project administration Matthew RisenHuber: conceptualization, formal analysis, methodology, funding acquisition, writing – review & editing William Munley: methodology Karen Noyes: conceptualization, funding acquisition, writing – review & editing Matt Douglas: conceptualization, project administration, funding acquisition, writing – review & editing Lori Metz: conceptualization, project administration, funding acquisition.

Conflicts of interest

There are no conflicts to declare.

Data availability

All data supporting the findings of this study are provided within the main article and the accompanying supplementary information (SI). Supplementary information: SI Fig. 1: image of the 3D printed column piece positioned in the 3D printed column holder with the 3D printed positive pressure piece attached to a compressed air line. SI Fig. 2: Hamilton setup for

microchemistry. SI Table 1: comprehensive characterization of standard reference materials (SRMs) and certified reference materials (CRMs) used in this study. SI Table 2: cup configuration for actinide measurements. SI Table 3: gravity-driven columns – sample information. SI Table 4: microchemistry – sample information. SI Table 5: dissolution experiments – sample information. See DOI: https://doi.org/10.1039/d6ja00127k.

Acknowledgements

The authors thank Tyler Sclieder and Robert Van Gundy for their thoughtful internal review of this manuscript. We also acknowledge the Pacific Northwest National Laboratory machine shop for making the custom-machined PTFE plates used in this study. We further acknowledge Chris DeGraaf and Linh Truong for their assistance with the preparation of figures. Research described in this manuscript is part of the Nuclear Forensics Transformational Initiative at Pacific Northwest National Laboratory conducted under the Laboratory Directed Research and Development Program at PNNL, a multiprogram national laboratory operated for the U.S. Department of Energy by Battelle Memorial Institute under contract number DE-AC05-76RL01830.

References

1 L. Metz, C. Beck, M. Douglas, J. Friese, S. Herman, K. Noyes and M. Zimmer, Nuclear Forensics: The Ultimate Analytical Chemistry Challenge, *Nucl. Sci. Eng.*, 2025, 1–12, DOI: 10.1080/00295639.2025.2592174.

2 G. J.-P. Deblonde, Biogeochemistry of Actinides: Recent Progress and Perspective, *ACS Environ. Au*, 2024, **4**(6), 292–306, DOI: 10.1021/acsenvironau.4c00037.

3 M. a. Denecke, N. Bryan, S. Kalmykov, K. Morris and F. Quinto, Sources and Behaviour of Actinide Elements in the Environment, in *Experimental and Theoretical Approaches to Actinide Chemistry*, John Wiley & Sons, Ltd, 2018, pp. 378–444, DOI: 10.1002/9781119115557.ch8.

4 Y. Faqir, Z. Li, T. Gul, Zahoor, Z. Jiang, L. Yu, C. Tan, X. Chen, J. Ma and J. Feng, Uranium's Hazardous Effects on Humans and Recent Developments in Treatment, *Ecotoxicol. Environ. Saf.*, 2025, **293**, 118043, DOI: 10.1016/j.ecoenv.2025.118043.

5 M. Raiwa, S. Büchner, N. Kneip, M. Weiß, P. Hanemann, P. Fraatz, M. Heller, H. Bosco, F. Weber, K. Wendt and C. Walther, Actinide Imaging in Environmental Hot Particles from Chernobyl by Rapid Spatially Resolved Resonant Laser Secondary Neutral Mass Spectrometry, *Spectrochim. Acta, Part B*, 2022, **190**, 106377, DOI: 10.1016/j.sab.2022.106377.

6 F. Quinto, R. Golser, M. Lagos, M. Plaschke, T. Schäfer, P. Steier and H. Geckeis, Accelerator Mass Spectrometry of Actinides in Ground- and Seawater: An Innovative Method Allowing for the Simultaneous Analysis of U, Np, Pu, Am, and Cm Isotopes below Ppq Levels, *Anal. Chem.*, 2015, **87**(11), 5766–5773, DOI: 10.1021/acs.analchem.5b00980.

7 B. D. Roach, E. K. Fenske, R. H. Ilgner, C. R. Hexel, T. J. Haverlock and J. M. Giaquinto, Development of a Fast and Efficient Analytical Technique for the Isotopic Analysis of Fission and Actinide Elements in Environmental Matrices, *J. Chromatogr.*, 2019, **1587**, 155–165, DOI: 10.1016/j.chroma.2018.12.029.

8 B. Schoene, C. Latkoczy, U. Schaltegger and D. Günther, A New Method Integrating High-Precision U–Pb Geochronology with Zircon Trace Element Analysis (U–Pb TIMS-TEA), *Geochim. Cosmochim. Acta*, 2010, **74**(24), 7144–7159, DOI: 10.1016/j.gca.2010.09.016.

9 M. Du and P. Thakur, Streamlining and Simplifying the Chemical Separation of Berkelium (^{249} Bk) from Other Actinides/Lanthanides and Fission Products, *ACS Omega*, 2025, **10**(25), 26756–26764, DOI: 10.1021/acsomega.5c01306.

10 S. Y. Han, B. J. Treves Brown, M. A. Higginson, P. Kaye, C. A. Sharrad and S. L. Heath, Development of an Automated Microfluidic System for Actinide Separation and Analysis, *J. Chromatogr.*, 2025, **1742**, 465646, DOI: 10.1016/j.chroma.2024.465646.

11 S. L. Maxwell Iii and V. D. Jones, Rapid Determination of Actinides in Urine by Inductively Coupled Plasma Mass Spectrometry and Alpha Spectrometry: A Hybrid Approach, *Talanta*, 2009, **80**(1), 143–150, DOI: 10.1016/j.talanta.2009.06.041.

12 J. E. Roane, T. A. DeVol, J. D. Leyba and R. A. Fjeld, The Use of Extraction Chromatography Resins to Concentrate Actinides and Strontium from Soil for Radiochromatographic Analyses, *J. Environ. Radioact.*, 2003, **66**(3), 227–245, DOI: 10.1016/S0265-931X(02)00109-1.

13 J. Stracke, P. Weßling, T. Sittel, C. Adam, F. Rominger, A. Geist and P. J. Panak, 2,6-Bis(5-(*Tert*-Butyl)-1*H*-Pyrazol-3-Yl)Pyridine: Effects of the Peripheral Aliphatic Side Chain on the Coordination of Actinides(III) and Lanthanides(III), *Inorg. Chem.*, 2024, **63**(29), 13214–13222, DOI: 10.1021/acs.inorgchem.4c00396.

14 C. Huang, H. Wang, L. Xie, L. Xu, S. Wu, Y. Yang and J. Yang, High-Precision Rb-Sr Isotope Analysis with Neoma MS/MS: Enhancing in Situ Geochronology by Laser Ablation, *Spectrochim. Acta, Part B*, 2025, **224**, 107117, DOI: 10.1016/j.sab.2025.107117.

15 N. X. Nie, R. Grigoryan and F. L. H. Tissot, High Precision Analysis of Potassium Stable Isotopes Using the Collision/Reaction Cell Neoma MC-ICPMS/MS, *J. Anal. At. Spectrom.*, 2024, **39**(8), 2038–2048, DOI: 10.1039/D4JA00133H.

16 S. R. Scott, K. P. Hobbs, A. D. French, I. J. Arnquist, S. Alcantar Anguiano, D. L. Sullivan and S. M. Herman, Uranium Isotopic Analysis in Unpurified Solutions by ICP-MS, *J. Anal. At. Spectrom.*, 2024, **39**(8), 2106–2115, DOI: 10.1039/D4JA00130C.

17 C. D. Standish, J. A. Milton, R. M. Brown and G. L. Foster, Matrix Independent and Interference Free *in Situ* Boron Isotope Analysis by Laser Ablation MC-ICP-MS/MS, *J. Anal. At. Spectrom.*, 2025, **40**(5), 1309–1322, DOI: 10.1039/D5JA00028A.

18 J. W. Grate, O. B. Egorov and S. K. Fiskum, Automated Extraction Chromatographic Separations of Actinides

Using Separation-Optimized Sequential Injection Techniques, *Analyst*, 1999, **124**(8), 1143–1150, DOI: 10.1039/a902579k.

19 S. C. Metzger, K. T. Rogers, D. A. Bostick, E. H. McBay, B. W. Ticknor, B. T. Manard and C. R. Hexel, Optimization of Uranium and Plutonium Separations Using TEVA and UTEVA Cartridges for MC-ICP-MS Analysis of Environmental Swipe Samples, *Talanta*, 2019, **198**, 257–262, DOI: 10.1016/j.talanta.2019.02.034.

20 S. J. Goldstein, A. A. Price, K. A. Hinrichs, S. P. Lamont, A. J. Nunn, R. S. Amato, A. M. Cardon and D. W. Gurganus, High-Precision Measurement of U-Pu-Np-Am Concentrations and Isotope Ratios in Environmental Reference Materials by Mass Spectrometry, *J. Environ. Radioact.*, 2021, **237**, 106689, DOI: 10.1016/j.jenvrad.2021.106689.

21 S. R. Scott, K. P. Hobbs, L. H. Hughes, I. J. Arnquist, T. D. Schlieder, D. L. Sullivan and A. D. French, Simultaneous analysis of U and Pu isotopes by MC-ICP-MS/MS purified CO_2, *Radioanal. Nucl. Chem.*, 2026, **335**(3), 2067–2077, DOI: 10.1007/s10967-025-10687-x.

22 E. P. Horwitz, R. Chiarizia, M. L. Dietz, H. Diamond and D. M. Nelson, Separation and Preconcentration of Actinides from Acidic Media by Extraction Chromatography, *Anal. Chim. Acta*, 1993, **281**(2), 361–372, DOI: 10.1016/0003-2670(93)85194-O.

